Electron transfer from a carbon nanotube into vacuum under high electric fields

2009 J. Phys.: Condens. Matter 21 195302

(http://iopscience.iop.org/0953-8984/21/19/195302)

J. Phys.: Condens. Matter **21** (2009) 195302 (9pp) doi:10.1088/0953-8984/21/19/195302

Electron transfer from a carbon nanotube into vacuum under high electric fields

L D Filip, R C Smith, J D Carey and S R P Silva

Nano Electronics Centre, Advanced Technology Institute, University of Surrey, Guildford, Surrey GU2 7XH, UK

E-mail: l.filip@surrey.ac.uk

Received 3 November 2008, in final form 17 February 2009
Published 7 April 2009
Online at stacks.iop.org/JPhysCM/21/195302

Abstract

The transfer of an electron from a carbon nanotube (CNT) tip into vacuum under a high electric field is considered beyond the usual one-dimensional semi-classical approach. A model of the potential energy outside the CNT cap is proposed in order to show the importance of the intrinsic CNT parameters such as radius, length and vacuum barrier height. This model also takes into account set-up parameters such as the shape of the anode and the anode-to-cathode distance, which are generically portable to any modelling study of electron emission from a tip emitter. Results obtained within our model compare well to experimental data. Moreover, in contrast to the usual one-dimensional Wentzel–Kramers–Brillouin description, our model retains the ability to explain non-standard features of the process of electron field emission from CNTs that arise as a result of the quantum behaviour of electrons on the surface of the CNT.

(Some figures in this article are in colour only in the electronic version)

1. Introduction

The field emission (FE) phenomenon was observed by Wood [1] more than one hundred years ago in his quest to produce x-rays more efficiently. The observation of the 'brilliant blue arcs' was at the time an unexpected outcome of the investigation. Thirty years later, scientific and technological developments focused the research towards the use of 'jets of electrons' exiting a metal surface when a strong electric field is applied. In this context, Fowler and Nordheim developed a theory to explain and understand the conditions in which FE can successfully be reproduced and harnessed [2]. The newly developed theory made use of the existing one-dimensional (1D) Wentzel–Kramers–Brillouin (WKB) description of the tunnelling phenomena and produced an exceptionally simple formula [2] for the emission current from a grounded cathode as a function of the applied potential (or as is most commonly used, the applied electric field) on the opposing anode. Technological advances at the end of the 20th century created yet another twist in the rapidly advancing research area on field emission. Creating efficient electron sources such as the Spindt tip arrays [3] and the discovery of large area techniques for depositing materials such as diamond and diamond-like carbon [4–7] paved the way for large area electronic applications. The unprecedented miniaturization of the electron sources and the discovery of new materials such as carbon nanotubes [8] (CNTs) generated new applications for field emission. While still preserving the exponential shape of the current–voltage (I–V) characteristics, which is the hallmark of tunnelling emission, some of the experiments performed on CNTs cannot be fully described within the Fowler–Nordheim (FN) theory. These include the observation of structured peaks in the measured emitted electron energy spectra [9–15] and the observation of ring shaped image patterns during emission [16–19] on individual CNTs as well as arrays of nanotubes.

The Fowler–Nordheim (FN) theory is a 1D description of the tunnelling process which is at the core of the field emission phenomenon. This theory was originally developed under assumptions, imposed on the emitting surface, of which at least two fail to be fulfilled in experiments [9–19] under realistic and practical conditions. The first approximation addresses the roughness of the emitting surface, which in the theory has to be perfectly flat and smooth. Real surfaces do not satisfy this assumption. In the case of a CNT the assumption is clearly violated as these structures are long cylinders usually terminated with a hemispherical cap of C atoms or possess a jagged edge of terminated C bonds for an uncapped CNT. The second approximation introduced in the FN theory requires that two of the geometric dimensions of the

emissive material extend indefinitely in the plane perpendicular to the tunnelling direction. By a simple kinetic argument the number of electrons incident on the potential barrier at the vacuum interface per unit time (or the so-called supply function) may be easily evaluated and by combining it with the WKB tunnelling probability, the FE current density can be easily derived. Such an approach proved to be very convenient for a wide range of metallic and semiconducting emitters, including the Spindt cathodes [3]. However, in the case of CNTs all the transverse geometric dimensions are shrunk to a nanometre scale, so that the subsequent quantum confinement effects can no longer be disregarded.

The main purpose of this article is the study of the electron transfer into vacuum exploring a quasi-free electron model. The CNT will be assumed to be a two-dimensional (2D) cylindrical manifold terminated smoothly with a hemisphere of the same radius. The electrons involved in the charge transport become 2D quasi-free objects bound to the surface of the CNT by a constant potential energy $-W_0$. The electronic states can then be found by solving the Schrödinger equation on the 2D manifold [20, 21] and the related electron densities on the CNT can be derived by assuming a Fermi–Dirac distribution over states. By combining these results with the standard 1D WKB approximation for the FE process, it was shown that the unusual experimental findings stated above are due to the quantization of the electron energy on the CNT [21]. Therefore, a more complete description of the FE process, from CNTs requires the consideration of the confinement quantization and reduced dimensionality when discussing the electron transfer into vacuum. For this reason, in order to go beyond the classical kinetic-plus-WKB description, one must rely on a more general definition for the emitted current [22]:

$$I(V) = e \sum_{\text{available states}} f(E_{\text{state}}) J_{\text{state}}(E_{\text{state}}, V), \qquad (1)$$

where e is the elementary charge and

$$f(E_{\text{state}}) = 2\left[1 + \exp\left(\frac{E_{\text{state}}}{k_{\text{B}}T}\right)\right]^{-1} \qquad (2)$$

is the Fermi–Dirac distribution function corrected for spin degeneracy, k_{B} is Boltzmann's constant and T is the overall temperature of the emitter. $J_{\text{state}}(E_{\text{state}}, V)$ is the total outgoing radial probability current of the electronic states in vacuum [23], which is the cornerstone of this approach. To compute the total outgoing radial probability current one has to describe the electron quantum dynamics in the 3D vacuum by accurately connecting it to the 2D behaviour on the CNT. The following sections introduce the framework for the proposed model. In section 2 a potential energy is defined in the space between the CNT cap and the anode, followed by the solutions of the Schrödinger equation on the 2D manifold and in the 3D vacuum in section 3. Section 4 introduces the new proposed emission current formula, while the results are discussed in section 5.

2. Defining the potential energy

In order to address the quantum mechanical problem of the electron transfer from the CNT into vacuum, the potential energy in the studied system has to be defined. It has already been assumed that the electrons are bound to the 2D surface of the CNT by a constant potential energy $-W_0$. The situation in vacuum however is more complicated to be easily described. One needs to find the potential energy in vacuum between the grounded CNT and a positively charged anode situated at some distance away. This electrostatic problem has been investigated through a number of methods in the literature [24–32]. However, due to its unexpected complexity, there is no definitive solution that could be used to describe the potential energy in the Schrödinger equation in vacuum. The result for the electrostatic problem to be presented in this work is to be viewed as a starting point for the more general problem of quantum tunnelling from nano-scale objects. More precisely the field emission model constructed using the potential energy obtained below is not dependent on a particular solution of the electrostatic problem but on one's ability to solve the 3D Schrödinger equation in vacuum.

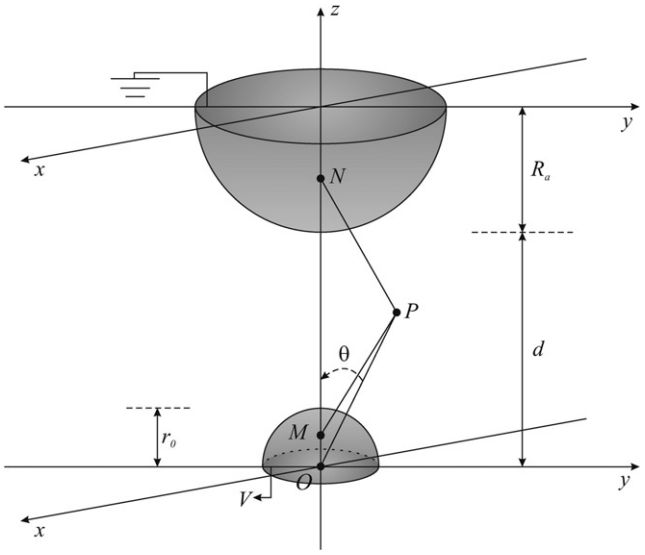

Figure 1. Sketch of the electrostatic model used to obtain the potential energy outside the CNT's cap (figure not drawn to scale).

The usual set-up for theoretical studies in the literature assumes an infinite planar anode thus differing slightly from the experimental reality where a spherical probe-anode is more commonly used for measurements of FE from single tips. To account for this practical configuration an electrostatic model has been developed in the present study based on the image charge method. The schematic of the proposed set-up is presented in figure 1. The anode is taken as a conductive sphere of radius R_{a} placed on the CNT axis, while the CNT cap is simplified to a grounded conducting sphere of radius r_0 ($R_{\text{a}} \gg r_0$), placed at a distance d away from the anode. Direct application of the image charge method to the grounded emitter on an infinite conductive plane facing an anode (regardless the shape) at a fixed positive voltage V would prove quite difficult. However, using information from the literature [30, 32] we have reversed the problem in the following manner: the cathode will be considered as grounded while the emitter connected to the cathode plane maintained at

a constant potential V. Once the electric field is obtained in the 'reversed' problem, the real electric field will simply have an opposite orientation:

$$\vec{E}_{\mathrm{P}}^{\mathrm{direct}} = -\vec{E}_{\mathrm{P}}^{\mathrm{inverse}} = \nabla_r V_{\mathrm{P}}^{\mathrm{inverse}}. \tag{3}$$

The charge distribution corresponding to the inversed configuration can be approximately replaced by a sequence of three collinear charges (figure 1). The charge at the origin O will generate the potential V on the emitter sphere:

$$q_{\mathrm{O}} = V r_0 4\pi\varepsilon_0 \tag{4}$$

and has an image q_{N} in the anode sphere:

$$q_{\mathrm{N}} = -q_0 \frac{R_{\mathrm{a}}}{d + R_{\mathrm{a}}}, \tag{5}$$

at the point N located $\frac{R_{\mathrm{a}}^2}{d+R_{\mathrm{a}}}$ away from its centre. In order to obtain a more accurate description of the charge distribution on the emitter's surface, an image of q_{N} with respect to this surface is also considered. The charge will be located at a point M at the distance $\frac{r_0^2}{d}\frac{d+R_{\mathrm{a}}}{d+2R_{\mathrm{a}}}$ away from O with:

$$q_{\mathrm{M}} = -q_{\mathrm{N}} \frac{r_0}{d} \frac{d + R_{\mathrm{a}}}{d + 2R_{\mathrm{a}}}. \tag{6}$$

The total potential at some arbitrary point P in vacuum at a distance r from the origin will be the superposition of potentials generated by the three individual charges. Taking into account that the FE process is highly dependent on the electric field strength in the first few nanometres outside the emitter cap, the formula for the electric potential must be accurate for distances r comparable to the radius r_0 of the emitter. By keeping only the terms of the second order in r/R_{a}, r_0/R_{a}, r/d and r_0/d, the potential in the reversed problem can be obtained in the following form:

$$V_{\mathrm{P}}^{\mathrm{inverse}}(r,\theta) = V\frac{r_0}{r}\left(1 + \frac{r_0}{d}\frac{R_{\mathrm{a}}}{d+2R_{\mathrm{a}}}\right) + V\frac{r_0^2}{d^2}\frac{R_{\mathrm{a}}(d+R_{\mathrm{a}})}{(d+2R_{\mathrm{a}})^2} \times \left(\frac{r_0^2}{r^2} - \frac{r}{r_0}\right)\cos\theta - V\frac{r_0}{d}\frac{R_{\mathrm{a}}}{d+2R_{\mathrm{a}}}. \tag{7}$$

The electric field in the 'direct' problem can now be retrieved through differentiation of equation (7) and by the use of equation (3). The corresponding potential energy in the neighbourhood close to the cathode follows from integration of the direct electric field along a radial path. In order to account for the non-electrostatic potential energy discontinuity at the CNT–vacuum interface it is required that the potential energy equals the vacuum barrier height χ of the CNT at $r = r_0$, for any value of the angle θ (see [27, 28, 33]). Thus, the potential energy formula to be used in the present approach of the electron tunnelling from a CNT into vacuum is given by:

$$W(r,\theta) = \chi + eV\left(1 + \frac{r_0}{d}\frac{R_{\mathrm{a}}}{d+R_{\mathrm{a}}}\right)\left(\frac{r_0}{r} - 1\right) - eV\frac{r_0^2}{d^2}\frac{R_{\mathrm{a}}(d+R_{\mathrm{a}})}{(d+2R_{\mathrm{a}})^2}\left(\frac{r}{r_0} - \frac{r_0^2}{r^2}\right)\cos\theta. \tag{8}$$

While rather involved, the above model still lacks the high sophistication of surface potentials barriers constructed for metals [34–36], which were backed by a substantial amount of experimental results. For the CNT case, where the study of individual tips is extremely difficult, not even the metallic character is always obvious. Therefore, while opened for further refinements, our model presently embeds other various contributions to the potential energy in the additive parameter χ. The extraction force $F_{\mathrm{extr}}(\theta)$ on the electron at the surface of the emitter can be evaluated by radial differentiation of equation (8) at $r = r_0$, which gives:

$$F_{\mathrm{extr}}(\theta) = \frac{eV}{r_0}\left(1 + \frac{r_0}{d}\frac{R_{\mathrm{a}}}{d+2R_{\mathrm{a}}}\right) + 3\frac{eV}{d}\frac{r_0}{d}\frac{R_{\mathrm{a}}(d+R_{\mathrm{a}})}{(d+2R_{\mathrm{a}})^2}\cos\theta. \tag{9}$$

One may note in equation (9) that the dependence on the elevation angle θ comes from a term that is essentially of the order of $(r_0/d)^2$. This means that, unless the anode is very close to the CNT's tip, the angular dependence of the extraction field may be negligible.

3. The quantum mechanical problem and solution of the Schrödinger equation

In order to produce numerical results that can be compared with existing measurement data, one should model the specific experimental set-up. As mentioned in the previous sections, the CNT is approximated by a strict 2D manifold where electrons behave as quasi-free particles. The manifold consists of a cylindrical sheet of length L and radius r_0 terminated smoothly by a hemispherical cap of the same diameter. The CNT's symmetry axis serves as the z-axis of the system pointing towards the vacuum and originating in the centre of the hemisphere. The position parameters on the CNT sheet are the angles of azimuth φ and elevation θ measured from the z-axis. The requirement of cylindrical symmetry for the electronic wavefunction is equivalent to imposing a restriction on the azimuth degree of freedom, such that the quasi-free electrons are confined in a one-dimensional (1D) potential energy well. For computational convenience, the origin of the energy scale is taken at the chemical potential of the quasi-free electron gas. Denoting by χ the CNT–vacuum barrier height and by W_0 the (position-independent) [37] energy of the bottom of the well, the total depth of the well appears to be $\chi - W_0$ (see figure 2). Thus, the quantity $|W_0|$ equals the chemical potential of the quasi-free electron gas as measured from the bottom of the well. Using this framework, the solution of the time independent Schrödinger equation on the CNT manifold has been obtained in [21] and takes the form:

$$\Psi_{l,m}^{\mathrm{2D}}(\theta,\varphi) = \alpha_{l,m}\Phi_m(\varphi)P_{l,m}(\cos\theta), \tag{10}$$

where $P_{l,m}(\cos\theta)$ represents the associated Legendre functions normalized in the interval [0,1] [38]. The indices $l = \overline{0,\infty}$ and $m = \overline{-l,l}$ are integers quantifying the electronic states on the CNT. The parameter $\alpha_{l,m}$ is obtained from the quantum mechanical connection requirements at the interface

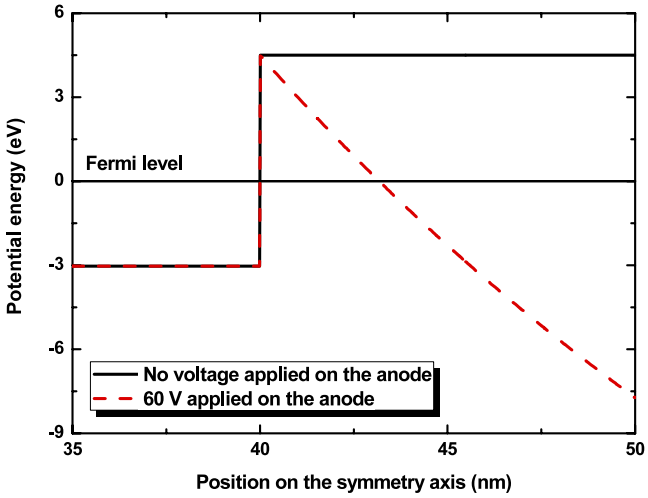

Figure 2. Potential energy diagram in vacuum for the 0 V applied on the anode case (black line) and 60 V applied (the red dashed line).

between the hemispherical cap and the cylindrical body and the normalization condition on the entire CNT. As a result of these requirements two different values for the parameter α emerge, depending upon the parity of the integer $l+m$ (for details on the parameter α see [21]). The remaining symbol in equation (10) is given by

$$\Phi_m(\varphi) = \frac{1}{\sqrt{2\pi}} e^{im\varphi}. \tag{11}$$

Having defined the potential energy in the close neighbourhood of the CNT tip in section 2, the tunnelling problem can now be addressed. Usually, this is approached by a 1D description, which is further oversimplified through the WKB approximation. The common FN equation is derived starting from such simplifying assumptions. In the present study, the Schrödinger equation will be solved in the full 3D vacuum space and the solutions will be connected to the corresponding solutions on the 2D CNT surface. Using the spherical coordinate system we have the following equation for the electron in the vacuum region:

$$-\frac{\hbar^2}{2m_0}\nabla^2\Psi_{\text{vacuum}}(r,\theta,\varphi) + W(r,\theta)\Psi_{\text{vacuum}}(r,\theta,\varphi) = E\Psi_{\text{vacuum}}(r,\theta,\varphi). \tag{12}$$

The above equation accounts for the full dimensionality of the vacuum electron. In the usual FN approaches, the multi-dimensional aspect of the electrons appears only in the statistics of the cathode's energy levels [39] and is normally described by a Fermi distribution.

One may attempt to solve equation (12) through the method of separating the variables. However, while the variable φ separates due to the cylindrical symmetry of the set-up, variables r and θ remain coupled through equation (8). By taking into account the observation at the end of the previous section regarding the θ-dependence of the extraction field, a further simplification can be applied to the potential energy: as the angular dependence is confined in a separate (normally very small) term of equation (8), it will be convenient to use the expression of the potential energy with $\theta = 0$. As will be shown in the next section, this does not mean that the current density is independent of the elevation angle. On the contrary, the θ-dependence of the emerging current density is quite consistent and comes from the corresponding variation of the wavefunction in vacuum.

Having made the above approximation, equation (12) separates into the angular and the radial part. Making use of the spherical coordinate system, the solutions for the angular equation are given by the spherical harmonics:

$$Y_{l,m}(\theta,\varphi) = \frac{1}{\sqrt{2\pi}} e^{im\varphi}\sqrt{\frac{1}{2l+1}\frac{(l+m)!}{(l-m)!}}P_{l,m}(\cos\theta)$$
$$\varphi \in [0, 2\pi], \quad \theta \in \left[0, \frac{\pi}{2}\right]. \tag{13}$$

Since the potential energy in equation (8) is approximated as independent on the value of the angle θ, the angular momentum can be considered as conserved for the electron when it shifts from the CNT into the vacuum region. Thus, the solution given by equation (13) will have the same integer index symbols l and m, as for the construction of the solution on the CNT cap in equation (10). Moreover, the transition of the electron from the CNT manifold into the vacuum is considered as an elastic process [40]. Consequently, the electron energy in the vacuum region will retain the same value on the CNT given by [21]:

$$E_l = -W_0 + \frac{\hbar^2}{2m^* r_0^2} l(l+1), \tag{14}$$

where m^* denotes the electron effective mass. The radial part $\Re(r)$ of the wavefunction can then be obtained through the following substitution [23] $u(r) = r\Re(r)$. This leads to the following 1D Schrödinger-like equation:

$$-\frac{\hbar^2}{2m_0}\frac{\mathrm{d}^2u(r)}{\mathrm{d}r^2} + W_l(r)u(r) = E_l u(r), \tag{15}$$

where

$$W_l(r) = W(r) + \frac{\hbar^2}{2m_0 r^2} l(l+1) \tag{16}$$

is an effective potential energy in the radial Schrödinger-like equation, and should not be confused with the real potential energy of the electron computed in the 3D vacuum region [23]. Analysing equations (8) and (16) reveals an almost linear behaviour of the effective potential energy in the close neighbourhood of the CNT cap as a function of the departure $r - r_0$ from the cap surface. An approximate solution in terms of Airy functions [38] can be found for equation (15) by expanding equation (16) in a power series around $r = r_0$ and retaining only the linear terms to give:

$$W_l(r) = -F_l(r - r_0) + \chi + \frac{\hbar^2}{2m_0}\frac{l(l+1)}{r_0^2}, \tag{17}$$

where

$$F_l = F_{\text{extr}}(0) + \frac{\hbar^2}{m_0}\frac{l(l+1)}{r_0^3}. \tag{18}$$

Using again the function change in equation (15) and the standard substitution for the Airy functions equation:

$$\xi_l(r) = -\left(\frac{2m_0}{\hbar^2 F_l^2}\right)^{1/3} [E_l - W_l(r)], \tag{19}$$

the following solution may be found for the radial equation:

$$\Re_l(r) = \frac{1}{r}[a_l Ai\,(\xi_l(r)) + b_l Bi(\xi_l(r))], \tag{20}$$

where a_l and b_l are constants to be determined and $Ai(x)$ and $Bi(x)$ are the Airy functions of the first and second kind, respectively [38].

The complete solution of equation (12) for the vacuum region near the CNT cap can now be written as

$$\Psi^{3D}_{l,m}(r,\theta,\varphi) = \sqrt{\frac{1}{2l+1}\frac{(l+m)!}{(l-m)!}} \times \frac{1}{r}[a_l Ai(\xi_l(r)) + b_l Bi(\xi_l(r))]\,\Phi_m(\varphi)P_{l,m}(\cos\theta)$$
$$r \in [r_0, d), \quad \theta \in \left[0, \frac{\pi}{2}\right], \quad \varphi \in [0, 2\pi]. \tag{21}$$

To summarize, in the first three sections of this paper, a 2D model for the CNT has been presented and the potential energy (equation (8)) in the 3D vacuum has been obtained using the image charge method. Using the method of separation of the variables the Schrödinger equation has been successfully solved after an approximation has been used on the potential energy, equation (17) with the full solution in the 3D vacuum given by equation (21). At this point the electron is defined both on the 2D manifold representing the CNT and also in the 3D vacuum outside the CNT cap. In order to address the problem of the electron transfer from the CNT into vacuum under the application an electric field, the two solutions need to be connected at the interface between the two media where the potential energy presents a discontinuity. It is in the following section that this issue is addressed and ultimately the FE current is obtained as an analytical formula.

4. The connection condition and the field emission current

As a dynamic process, the extraction of electrons from a material under the influence of a high electric field can be regarded as unidirectional, i.e. once emitted, the probability for the electron being recaptured by the emitter can be neglected. Therefore, the solution of the Schrödinger equation in vacuum given by equation (21) is to satisfy the radiating boundary condition [40–42] in the neighbouring vacuum. The condition requires that the radial component of the current density is purely outgoing (i.e. strictly positive). The radial component of the probability current density is defined as [23]:

$$j_r = \frac{\hbar}{m_0}\,\mathrm{Im}\left(\Psi^* \frac{\partial \Psi}{\partial r}\right). \tag{22}$$

Applying the above definition to the solution of the Schrödinger equation given by equation (21) and conveniently rearranging the terms, one finds

$$j_r^{l,m}(r,\theta) = \frac{1}{4\pi^2 r^2}\left(\frac{\hbar F_l}{4m_0^2}\right)^{1/3} \frac{\left[P_{l,m}(\cos\theta)\right]^2}{2l+1}\frac{(l+m)!}{(l-m)!} \times \left(|a_l + \mathrm{i}b_l|^2 - |a_l - \mathrm{i}b_l|^2\right). \tag{23}$$

It is now clear that the radial component of the probability current density vector is purely outgoing when

$$a_l = \mathrm{i}b_l, \tag{24}$$

leaving only one undetermined coefficient in equation (21). In order to remove this last indeterminacy one can connect the solutions of the Schrödinger equation on the CNT manifold to their 3D counterparts in the vacuum. As the rate of the CNT-to-vacuum transfer is normally rather small, it will be considered that the electron wavefunction is concentrated mainly onto the CNT. The solutions on the CNT are normalized; therefore a straightforward computation will reveal a vanishing axial probability current on the CNT. It is now clear that a smooth connection between the solution on the CNT and the one in vacuum would have as a result a null probability current in vacuum and by virtue of equation (1) no field emission current. This is unrealistic and incorrect. Similar conclusions have been previously reported in the literature in relation to the electron transfer from a two-dimensional electron gas (2DEG) into a continuum [40]. Accurate calculations of the current were obtained by a simpler requirement of the continuity of the localization probability density. We adopt in our study this approach and we modify the continuity condition in order to adapt it to the dimensionality change between the two environments of the 2D CNT and the 3D vacuum. It is therefore assumed that if the electron is essentially spread on the 2D CNT cap before emission and immediately after emission will expand into a hemispherical shell whose thickness is a certain fraction λ (a dimensionless parameter) of r_0. The localization probability of an electron on an infinitesimal area element dS on the CNT cap before emission is $|\Psi^{2D}_{l,m}|^2\,\mathrm{d}S$ and $|\Psi^{3D}_{l,m}|^2\,\mathrm{d}V$ is the localization probability in a volume $\mathrm{d}V$ in vacuum, immediately outside the surface of the CNT cap after emission. According to the previous hypothesis, we have: $\mathrm{d}V = \lambda r_0\,\mathrm{d}S$. By further assuming that the localization probability is conserved in the transfer from $\mathrm{d}S$ to $\mathrm{d}V$, one may write:

$$|\Psi^{2D}_{l,m}(\theta,\varphi)^2| = \lambda r_0 |\Psi^{3D}_{l,m}(r_0,\theta,\varphi)|^2. \tag{25}$$

Equation (25) relates the initial 2D spread of the electron on the CNT cap to a 3D volume outside the CNT by a factor λr_0 and thus λ can be viewed as a *localization* parameter.

Combining equations (24) and (25) we can evaluate the undetermined constants a_l and b_l in equation (21) as functions of the localization parameter λ. Thus, the total probability current carried by $\Psi^{3D}_{l,m}$ towards the anode can now be obtained through integration of $j_r^{l,m}(r,\theta)\,\mathrm{d}S$ over the CNT's hemispherical cap:

$$J_{l,m} = \frac{2}{\lambda}\left(\frac{\hbar F_l}{4m_0^2}\right)^{1/3} \frac{\alpha^2_{l,m} r_0}{\pi\left[Ai^2(\xi_l(r_0)) + Bi^2(\xi_l(r_0))\right]}. \tag{26}$$

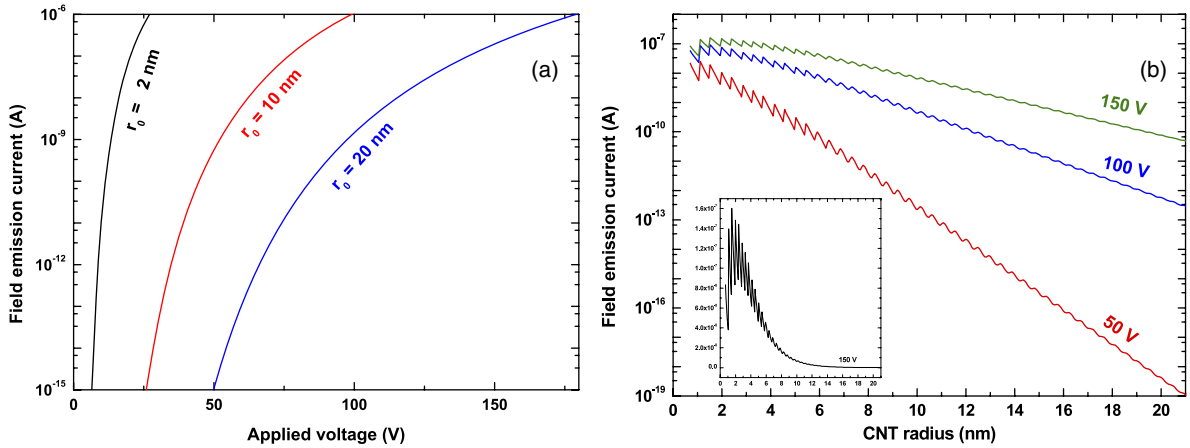

Figure 3. (a) Field emission current as a function of the anode applied voltage, calculated for three values of the CNT radius. (b) Field emission current as a function of the CNT radius calculated for three anode voltages. The inset shows the linear scale for the case of 150 V anode voltage, revealing the pronounced maximum at lower CNT radii.

Using equation (1), the field emission current can now be obtained from the summation over the contribution of all the (l, m) states on the CNT to the tunnelling process:

$$I = e\frac{2r_0}{\pi\lambda}\sum_{l=0}^{\infty}\left(\frac{\hbar F_l}{4m_0^2}\right)^{1/3}\frac{f(E_l)}{\left[Ai^2\left(\xi_l(r_0)\right)+Bi^2\left(\xi_l(r_0)\right)\right]} \times \sum_{m=-l}^{l}\alpha_{l,m}^2. \tag{27}$$

5. Results and discussion

The theoretical model presented in the previous sections aim to provide a deeper understanding of the electron field emission process. The newly introduced framework shifts the importance of the purely electrostatic argument governing the Fowler–Nordheim description of field emission from CNTs onto the electronic structure of the emitter itself and its crucial role played in the emission process. The results to be presented in this section analyse the response of the proposed model with the variation of structural and functional parameters of the whole emission set-up.

Typical field emission experiments, where single emitters are exposed to a high electric field by means of a neighbouring anode, have the experimental data plotted in the common current versus voltage (I–V) characteristics. Figure 3(a) shows the calculated field emission current for three CNTs of radii 2, 10 and 20 nm respectively using equation (27). As is can be seen in figure 3(a), our model predicts the rapid increase of the output current for smaller tube diameters, which is due to the increase of the extraction force. Such an increase can be explained as the extraction force in equation (9) is inversely proportional with the radius of the CNT r_0, thus resulting in a thinner potential barrier and therefore a higher emission current.

An important feature of FE from CNTs that cannot be systematically analysed experimentally is the variation of the FE current with the radius of the emitter. The FE formula given by equation (27) allows one to consider a continuous range of radii, within the experimentally plausible values for CNTs, and to study such a variation for different values of the applied voltage. Figure 3(b) shows the current versus radius dependence for three values of the applied anode voltage. As it can be seen, the model predicts the increase of the FE current as the anode voltage is increased for the same radius of the emitter. However the model also reveals a hidden aspect of emission specific to CNTs: the appearance of high frequency oscillations of the current, the magnitude of which increases for smaller diameter values (see inset of figure 3(b)). The existence of such a maximum is explained by the balance between two opposite effects induced by the decrease of the CNT radius: the extraction force in equation (9) increase as the CNT radius decreases which will increase the emission current and the lowering of the electron density on the CNT cap, which will tend to decrease the emitted current. The oscillations in figure 3(b) are consequences of the constraints imposed by the connection conditions at the boundary between the cylindrical body of the CNT and the spherical cap.

A practically important discussion of the model's response would be the study of the influence of the CNT tip to anode separation on the FE current. Such experiments have already been performed previously [43–49], in various arrangements and for a wide range of separation distances. Our model allows for consideration of a continuous range of tip to anode separations and the study of the FE process for the more delicate situations where the magnitude of the barrier is affected by the position of the anode itself. Figure 4 shows such a study where the FE current was plotted against the CNT tip-to-anode distance for three applied voltages. As it can be seen, there is a strong dependence of the current when the separation is smaller than 100 nm and then the current is stabilized for the rest of the range. This trend is to be expected as the anode strongly influences the vacuum barrier at the tip of the CNT when it is brought into the close neighbourhood, a fact that is in good agreement with a number of experiments [43, 44].

The FE formula presented in equation (27) allows one to study various scenarios involving the geometrical parameters discussed above. However, the model also includes parameters

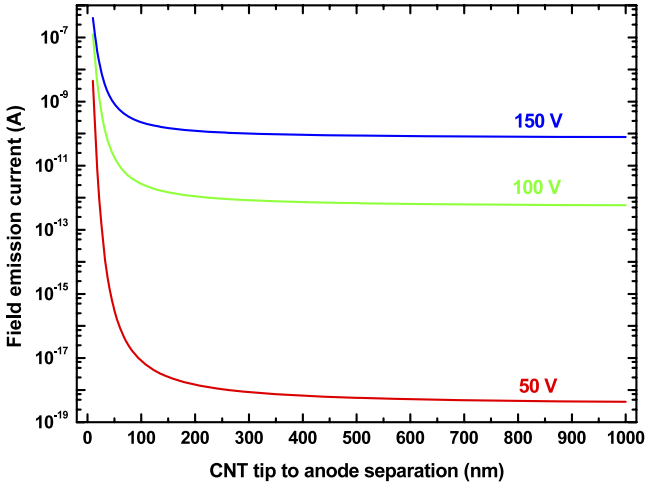

Figure 4. Field emission current as a function of the CNT tip to anode separation calculated for three applied voltages.

related to the electronic behaviour of the CNT–vacuum interface. These are the vacuum barrier height χ and the localization parameter λ. The influence of these two parameters on the FE current is illustrated in figures 5(a) and (b). The electron emission process occurs when the value of the local extraction field is comparable to the electron bonding fields in atoms. It is thus expected a major change in the vacuum barrier height when strong fields are applied to the CNT–vacuum interface [50], or when other physical conditions at the interface change. To consider such situations, it is useful to assume the vacuum barrier height, χ, as an adjustable parameter. Figure 5(a) shows the emitted current as a function of χ for three values of the applied anode voltage. For all three cases, a strong decrease of the FE current can be observed as the vacuum barrier height is increased. This expected behaviour is clearly related to the decrease in transparency for thicker vacuum barriers. The dependence of the FE current on the localization parameter λ is depicted in figure 5(b) for three values of the applied anode voltage. As shown in section 4, the localization parameter quantifies the spread of the just emitted electron in the neighbouring vacuum as compared to its localization on the CNT cap. This is an important result, as it shows the decrease of the FE current when the localization of the emitted electrons is lower (or the delocalization is higher). A lower λ value means a higher localization of the just emitted electron into the vacuum, therefore a lower spread along its way toward the anode. This would therefore lead to a higher current density. On the other hand a larger value for λ would imply a broader spread of the just emitted electron into the vacuum and a smaller value of the current density. The results shown in figure 5(b) confirm the model's expectations and show a sharp decrease of the FE current for the high-localization range and a saturation tendency towards low-localization regime.

The studies presented so far are entirely qualitative in order to show how the proposed FE model is influenced by the geometrical and electronic parameters characteristic to the system studied. However, if real experimental FE data are available, the model can be used to fit such data. Smith *et al* have performed an elaborate FE experiment from a single CNT, using a nano-manipulation system inside a scanning electron microscope (SEM) chamber. The full details of the experiment can be found in [45]. In figure 6 the FE model presented here was used to fit the experimental data in [45]. The main parameters used for the fit were the vacuum barrier height χ and the localization parameter λ. In figure 5(a) it was shown that the vacuum barrier height strongly influences the FE current for different values of the applied anode voltage. The available experimental data were collected for different CNT tip to anode separations, thus different values of the applied voltages were applied each time in order to obtain the maximum current of 1 μA set as a limit during the experiment to protect the sample. For this reason, different best-fit values of the vacuum barrier height χ were obtained for each separation. Best-fit values for both parameters are summarized in the table attached to figure 6. A decreasing tendency of χ with decreasing d is observed, which looks normal for the present theoretical context and may be related qualitatively to previous independent predictions [36]. On the contrary, the variation of the localization parameter λ,

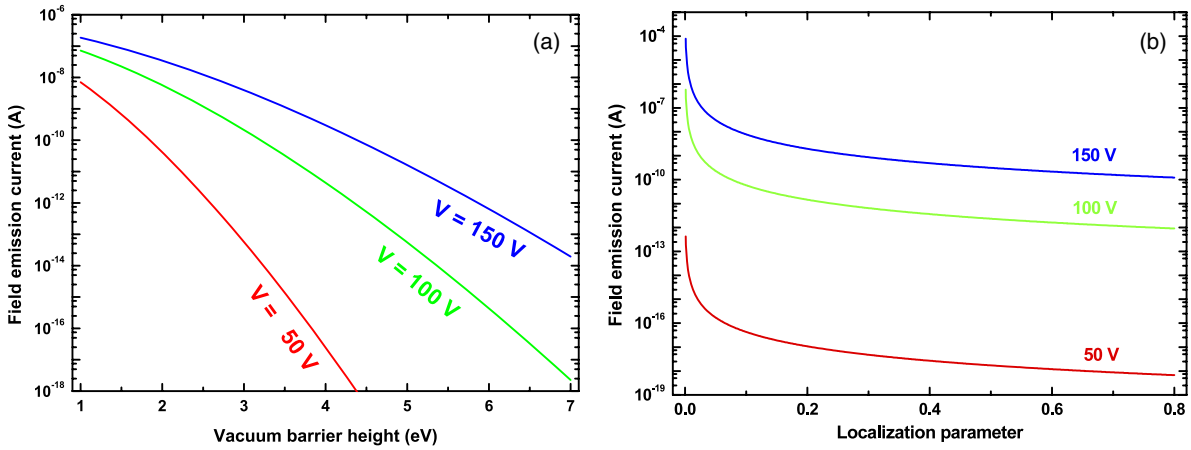

Figure 5. (a) Field emission current as a function of the vacuum barrier height χ calculated for three values of the applied voltage. (b) Field emission current as a function of the localization parameter λ calculated for three values of the applied voltage.

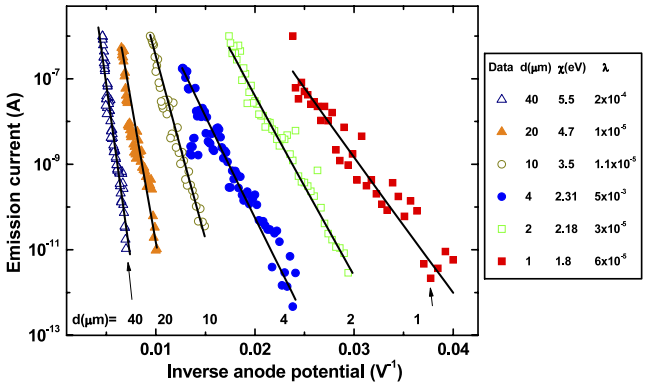

Figure 6. Experimental field emission data (scattered symbols) fitted with the proposed model (continuous lines). The values for the best-fit parameters are shown in the attached table. The anode radius was $R_a = 5$ μm and a common value of 3.033 eV has been used for W_0.

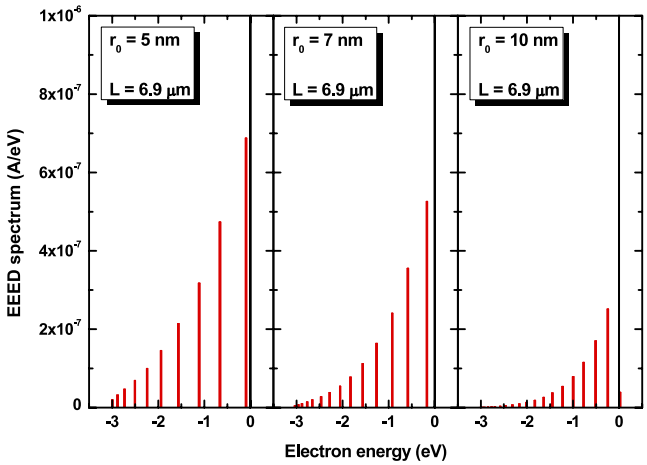

Figure 7. The emitted electron energy distribution (EEED) spectra calculated for three values of the CNT radius r_0.

which acts as a scaling factor for the overall fit, shows a quite erratic aspect that could be linked to the inherent experimental noise. Although this might suggest that a constant value for λ should be expected, only using data from improved experimental techniques may draw a definite conclusion. The value of the parameter W_0 has been tuned such that the work function obtained from fitting the experimental data taken at a large CNT-anode separation is in a normal range for CNTs (around 5 eV). It turned out that the best fit was possible only for large values of W_0, suggesting that the CNT behaviour resembles that of a metallic needle. We have therefore set this parameter to the value of 3.033 eV, corresponding to the nearest neighbour transfer integral for a 1D chain of carbon atoms in polyethylene [51]. While in the literature there are computations that place the Fermi level below the 'conduction band minimum' [52], previous studies indicate both theoretically [53, 54] and experimentally [55, 56] that there are plenty of circumstances when CNTs behave as metallic conductors.

Another investigation technique, specific for materials with field emission properties, is the measurement of the emitted electron energy distribution spectrum or EEED. The usual trend of these spectra for bulk materials is a continuous curve with a pronounced peak about the Fermi level (provided that the origin for the energy scale was set at the Fermi level). At 0 K the entire emission takes place from below the Fermi level as electrons cannot populate the energy states above. Thus the EEED spectra will be entirely confined below the Fermi level. At higher temperatures the electrons will be able to populate higher energy states due to thermal excitation and the EEED will show a tail above the Fermi level. However, as the emissive materials are shrunk down to the nano-scale the quantization of the electron inside a nano-sized particle or object will greatly influence the shape of these spectra. Recent EEED experiments performed by Lobanov and Sheshin on sharp CNTs [15] revealed a fine structure embedded in the spectrum. This peculiar behaviour of the CNTs was attributed to the competition between the availability of allowed energy states on the CNT cap and their statistical occupancy. Instead of a continuous spectrum as obtained from a bulk metal, where all the energy levels are occupied up to the Fermi level, the CNTs appear to have forbidden energy states which are unoccupied by electrons thus generating the fine structure in the EEED [15]. A similar fine structure in the EEED can be obtained in the presented model. A study of the influence of the CNT radius r_0 and length L on the EEED spectrum is presented in figure 7. While not being a quantitative study, the fine structure is clearly exemplified in this figure for three different radii. The change in radius of the CNT dramatically influences the fine structure and the overall magnitude of the spectrum as the density of the energy levels given by equation (14) is inversely proportional to the square of the CNT radius. Thus, the smaller the radius the closer to the Fermi level the energy levels given by equation (14) will be and the more intense will be their participation to the emission process (provided that the energy state is allowed by the quantization rules [21]). For a larger CNT radius, the energy levels will be further away from the Fermi level thus having a considerably lower probability to participate in the emission process.

6. Conclusion

A new description of electron emission has been proposed by direct calculation of the solution of the 2D Schrödinger equation on the CNT surface and a 3D solution in vacuum in which a weak connection condition is used to account for the change in dimension between the 2D surface of the CNT and the 3D vacuum. The probability current was calculated at the surface of the CNT and by assuming a Fermi–Dirac electron statistics on the CNT, the field emission current was calculated as a sum over all energies from the product between the electron charge, the electron statistics and the probability current. The proposed model was then investigated in a series of studies in order to test the influences of the various geometrical and electronic parameter used throughout on the FE current. The results were discussed and qualitatively compared with known experimental conclusions already existent in the literature. It was shown that the model

is able to qualitatively replicate a large number of experimental results and, if FE experimental data are available, it can be used to fit the obtained data.

Acknowledgment

The authors would like to thank EPSRC for sponsoring this work with the award of a Portfolio Partnership grant to the University of Surrey.

References

[1] Wood R W 1897 *Phys. Rev.* I **5** 1
[2] Fowler R H and Nordheim L 1928 *Proc. R. Soc.* A **119** 173
[3] Spindt C A, Brodie I, Humphrey L and Westerberg E R 1976 *J. Appl. Phys.* **47** 5248
[4] Okano K, Yamada T, Sawabe A, Koizumi S, Itoh J and Amaratunga G A J 2001 *Appl. Phys. Lett.* **79** 275
[5] She J C, Xu N S, Huq S E, Deng S Z and Chen J 2002 *Appl. Phys. Lett.* **81** 4257
[6] Silva S R P, Amaratunga G A J and Okano K 1999 *J. Vac. Sci. Technol.* B **17** 557
[7] Xu N S and Huq S E 2005 *Mater. Sci. Eng.* R **48** 47
[8] Iijima S 1991 *Nature* **354** 56
[9] Latham R V and Wilson D A 1983 *J. Phys. D: Appl. Phys.* **16** 455
[10] Dean K A, Groening O, Kuttel O M and Schlapbach L 1999 *Appl. Phys. Lett.* **75** 2773
[11] Fransen M J, van Rooy T L and Kruit P 1999 *Appl. Surf. Sci.* **146** 312
[12] Groning O, Kuttel O M, Emmenegger C, Groning P and Schlapbach L 2000 *J. Vac. Sci. Technol.* B **18** 665
[13] de Jonge N and van Druten N J 2003 *Ultramicroscopy* **95** 85
[14] Oshima C, Matsuda K, Kona T, Mogami Y, Yamashita T, Saito Y, Hata K and Takakura A 2003 *J. Vac. Sci. Technol.* B **21** 1700
[15] Lobanov V M and Sheshin E P 2006 *Tech. Phys. Lett.* **32** 1074
[16] Dean K A and Chalamala B R 2000 *Appl. Phys. Lett.* **76** 375
[17] Saito Y and Uemura S 2000 *Carbon* **38** 169
[18] Saito Y, Hata K, Takakura A, Yotani J and Uemura S 2002 *Physica* B **323** 30
[19] Dean K A and Chalamala B R 2003 *J. Vac. Sci. Technol.* B **21** 868
[20] Filip L D, Nicolaescu D, Tanemura M, Kanemaru S and Itoh J 2005 *J. Vac. Sci. Technol.* B **23** 649
[21] Filip L D, Nicolaescu D and Silva S R P 2006 *J. Vac. Sci. Technol.* B **24** 874
[22] Magnus W and Schoenmaker W 2002 *Quantum Transport in Submicron Devices. A Theoretical Introduction* (Berlin: Springer)
[23] Gottfried K and Yan T-M 2003 *Quantum Mechanics: Fundamentals* (New York: Springer)
[24] Brodie I and Schwoebel P R 1994 *Proc. IEEE* **82** 1006
[25] Mollicone M M, Dacal L C O and de Castilho C M C 1996 *Appl. Surf. Sci.* **94/95** 68
[26] Kokkorakis G C, Modinos A and Xanthakis J P 2002 *J. Appl. Phys.* **91** 4580
[27] Edgcombe C J 2003 *Ultramicroscopy* **95** 49
[28] Edgcombe C J and Johansen A M 2003 *J. Vac. Sci. Technol.* B **21** 1519
[29] Read F H and Bowring N J 2004 *Nucl. Instrum. Methods* A **519** 305
[30] Wang X Q, Wang M, He P M, Xu Y B and Li Z H 2004 *J. Appl. Phys.* **96** 6752
[31] Smith R C, Carey J D, Forrest R D and Silva S R P 2005 *J. Vac. Sci. Technol.* B **23** 632
[32] Wang X Q, Wang M, Li Z H, Xu Y B and He P M 2005 *Ultramicroscopy* **102** 181
[33] Edgcombe C J 2005 *Phys. Rev.* B **72** 045420
[34] Cutler P H and Gibbons J J 1958 *Phys. Rev.* **111** 394
[35] Hartman R L, Mackie W A and Davis P R 1996 *J. Vac. Sci. Technol.* B **14** 1952
[36] Jensen K L, Feldman D W and O'Shea P G 2005 *J. Vac. Sci. Technol.* B **23** 621
[37] Filip V, Nicolaescu D, Tanemura M and Okuyama F 2004 *J. Vac. Sci. Technol.* B **22** 1234
[38] Abramowitz M and Stegun I A 1974 *Handbook of Mathematical Functions with Formulas, Graphs and Mathematical Tables* (New York: Dover)
[39] Jensen K L 2001 *Vacuum Microelectronics* ed W Zhu (New York: Wiley–Interscience) p 33
[40] Filip V, Nicolaescu D, Wong H, Nagao M and Chu P L 2005 *J. Vac. Sci. Technol.* B **23** 657
[41] Gamow G 1928 *Nature* **122** 805
[42] Razavy M 2003 *Quantum Theory of Tunnelling* (New Jersey: World Scientific)
[43] Kuzumaki T, Takamura Y, Ichinose H and Horiike Y 2001 *Appl. Phys. Lett.* **78** 3699
[44] Kuzumaki T, Horiike Y, Kizuka T, Kona T, Oshima C and Mitsuda Y 2004 *Diamond Relat. Mater.* **13** 1907
[45] Smith R C, Cox D C and Silva S R P 2005 *Appl. Phys. Lett.* **87** 103112
[46] Wang M S, Peng L M, Wang J Y, Jin C H and Chen Q 2006 *J. Phys. Chem.* B **110** 9397
[47] Hii K F, Vallance R R, Chikkamaranahalli S B, Menguc M P and Rao A M 2006 *J. Vac. Sci. Technol.* B **24** 1081
[48] Kim C D, Jang H S, Lee S Y, Lee H R, Roh Y S, Rhee I S, Lee E W, Yang H S and Kim D H 2006 *Nanotechnology* **17** 5180
[49] Asaka K, Nakahara H and Saito Y 2008 *Appl. Phys. Lett.* **92** 023114
[50] Jensen K L and Ganguly A K 1993 *J. Vac. Sci. Technol.* B **11** 371
[51] Saito R, Dresselhaus G and Dresselhaus M S 1998 *Physical Properties of Carbon Nanotubes* (London: Imperial College Press)
[52] Ayuela A, Chico L and Jaskolski W 2008 *Phys. Rev.* B **77** 085435
[53] Mintmire J W, Dunlap B I and White C T 1992 *Phys. Rev. Lett.* **68** 631
[54] Hamada N, Sawada S and Oshiyama A 1992 *Phys. Rev. Lett.* **68** 1579
[55] Carroll D L, Redlich P, Ajayan P M, Charlier J C, Blase X, DeVita A and Car R 1997 *Phys. Rev. Lett.* **78** 2811
[56] Petit P, Mathis C, Journet C and Bernier P 1999 *Chem. Phys. Lett.* **305** 370